EPJ B
Condensed Matter and Complex Systems
EPJ.org
your physics journal

Eur. Phys. J. B (2017) 90: 108 DOI: 10.1140/epjb/e2017-70597-6

The electrical conductance growth of a metallic granular packing

Zorica M. Jakšić, Milica Cvetković, Julija R. Šćepanović, Ivana Lončarević, Ljuba Budinski-Petković and Slobodan B. Vrhovac

edp sciences
Società Italiana di Fisica
Springer

Eur. Phys. J. B (2017) 90: 108
DOI: 10.1140/epjb/e2017-70597-6

THE EUROPEAN PHYSICAL JOURNAL B

Regular Article

The electrical conductance growth of a metallic granular packing

Zorica M. Jakšić[1], Milica Cvetković[1], Julija R. Šćepanović[1], Ivana Lončarević[2], Ljuba Budinski-Petković[2], and Slobodan B. Vrhovac[1,a]

[1] Institute of Physics Belgrade, University of Belgrade, Pregrevica 118, 11080 Zemun, Belgrade, Serbia
[2] Faculty of Engineering, Trg D. Obradovića 6, 21000 Novi Sad, Serbia

Received 7 October 2016 / Received in final form 12 March 2017
Published online 14 June 2017 –

Abstract. We report on measurements of the electrical conductivity on a two-dimensional packing of metallic disks when a stable current of ∼1 mA flows through the system. At low applied currents, the conductance σ is found to increase by a pattern $\sigma(t) = \sigma_\infty - \Delta\sigma E_\alpha[-(t/\tau)^\alpha]$, where E_α denotes the Mittag-Leffler function of order $\alpha \in (0, 1)$. By changing the inclination angle θ of the granular bed from horizontal, we have studied the impact of the effective gravitational acceleration $g_{\text{eff}} = g \sin\theta$ on the relaxation features of the conductance $\sigma(t)$. The characteristic timescale τ is found to grow when effective gravity g_{eff} decreases. By changing both the distance between the electrodes and the number of grains in the packing, we have shown that the long term resistance decay observed in the experiment is related to local micro-contacts rearrangements at each disk. By focusing on the electro-mechanical processes that allow both creation and breakdown of micro-contacts between two disks, we present an approach to granular conduction based on subordination of stochastic processes. In order to imitate, in a very simplified way, the conduction dynamics of granular material at low currents, we impose that the micro-contacts at the interface switch stochastically between two possible states, *"on"* and *"off"*, characterizing the conductivity of the micro-contact. We assume that the time intervals between the consecutive changes of state are governed by a certain waiting-time distribution. It is demonstrated how the microscopic random dynamics regarding the micro-contacts leads to the macroscopic observation of slow conductance growth, described by an exact fractional kinetic equations.

1 Introduction

The electrical resistance of a granular packing is a combination of the individual resistances of both the grains and the contacts between them [1]. Such a combination is a strong function of global properties concerning the grain assembly (packing size and density, external loads) and local properties at the contact scale of two grains (surface state, roughness, degree of oxidation, presence of impurities). Understanding the electrical conduction through real granular materials is a complicated many body problem since particles may have simultaneously broad distributions of sizes and strongly varying morphologies.

The main contribution to the overall conductivity of the packing of metallic grains comes from the contact resistances, which may have two origins: tunneling [2] and constrictions [3]. The tunneling resistances may have very high values, but especially concern metallic powders coated by thin oxide film. On the other hand, constriction resistances are due to the narrowness of the conducting path owing to the small contact area between two particles. Actually, any contact is made of a number of touching points rather than by well-defined surface.

[a] e-mail: vrhovac@ipb.ac.rs

Experiments on the electrical properties of granular systems have been performed in the past. In 1890, Branly [4] discovered the extreme sensitivity of the conductivity of metal filling to an electromagnetic wave. The Branly's effect is an instability of the electrical conductance that appears in oxidized granular metallic material under mechanical loading [5–9]. Electrical conduction within metallic granular packings displays other interesting properties. Indeed, in both 1D and 2D granular systems at low current, the wide distribution of contact resistances results in a logarithmic behavior for the voltage/current characteristics [10]. At high enough current, the voltage saturates due to the local welding of micro-contacts between grains [11]. Furthermore, electrical conduction shows a large sensitivity on the small mechanical and thermal perturbations of the packing [12,13]. Origin of these large non-Gaussian conductance fluctuations should be found in local micro-contact rearrangements at each grain rather than collective rearrangements of grains inside the packing.

Although many experiments have been performed for studying electrical aspects of granular matter, only few reports [14,15] can be found for describing the temporal evolution of the electrical resistance $R(t)$ in packing

of metallic grains when a stable current flows through the system. Dorbolo et al. [14] measured the electrical resistance in a 2D system and found that the decay process in the case of injected currents $35 \lesssim I \lesssim 50$ mA may be decomposed into three phases. At first the resistance decreases during the first minute, after that the curves $R(t)$ are stabilized during $\sim 10^3$ s before decreasing again. However, for lower injected currents $10 \lesssim I \lesssim 25$, the resistance $R(t)$ is a monotonically decreasing function. It would be interesting to find out where such unusual behavior comes from. Dorbolo et al. [14] suggested that the long term decay of the electric resistance $R(t)$ seems to be related to the enhancement of contacts themselves. The aim of this work is to investigate the regime of very small electric currents $I \sim 1$ mA in order to gain a better understanding the origin of the slow electrical resistance relaxation in granular packing.

We focus on the electrical transport within 2D packing of metallic disks directly connected to an electrical source. A fixed current has been injected during a few hours and conductance $\sigma(t) = 1/R(t)$ has been recorded at regular intervals. Experiments were performed for two different inclination angles θ of the granular bed from horizontal. Consequently, we have considered the impact of the effective gravitational acceleration $g_{\text{eff}} = g \sin\theta$ on the relaxation features of the conductance $\sigma(t)$. We could change the distance between the electrodes, i.e. the number of grains in the packing. In this way we were able to compare the influence of large force chain rearrangements with impact of local micro-contact rearrangements at each disk on overall electrical conductivity of the packing.

We have tried to fit different functional forms to the slow temporal relaxation of $\sigma(t)$ obtained in the experiments, looking in particular at the relaxation functions proposed in the experimental and numerical studies of disordered systems [16]. We have found that the most suitable functional form for our experimental data is the Mittag-Leffler law (1) (corresponding mathematical definitions are provided later in the text; see Eqs. (2) and (3)). The main question that needs an answer is whether equation (1) represents only a convenient fitting expression or it has a more fundamental meaning, associated to some peculiar dynamical events which are dominant in the conductance relaxation. We would like to elucidate this point more thoroughly in order to develop a dynamic model for the electric contact between two grains based on the stochastic fractional process that captures this relaxation dynamics.

A typical rough surface of metallic grain may include many small contacts of varying sizes. Our model assumes the electrical current flow is between two contiguous bulk conducting materials and the current flows through the conducting a-spots or constrictions (micro-contacts) [3]. The model does not explicitly account for quantum effects or the spreading resistance resulting from the thin film micro-contacts. Our approach is based on the probabilistic formalism of limit theorems which provides tools to relate the non-differentiable nature of microscopic dynamics of components in complex systems to the macroscopic description of such systems in the form of fractional operators [17–20]. We suppose that there are only two possible states of micro-contacts, referred to as *"switched on"* and *"switched off"*. In order to imitate, in a very simplified way, the relaxation features of conductance $\sigma(t)$ under low currents, we impose that the micro-contacts at interface switch stochastically between two possible states. Starting with the description of the two-state system evolution as a Markovian process, we develop the analysis on a subordinated random process. The process differs from the Markovian ones by the temporal variable becoming random [19]. This generalization is of a stochastic origin and produces the fractional operator in the resulting evolution equation for the conductance. The evolution equation is capable of reproducing a wide range of experimental behavior.

In the following section, we present the experimental set-up and describe the experimental procedures. The experimental results are reported and discussed in Section 3. Definition of the model and discussion on the physical interpretation of the model parameters are given in Section 4. In the same section results of numerical simulation are presented, discussed, and wherever possible compared with analytical results. Finally, we summarize our findings in Section 5.

2 Experiment

Let us now describe our experimental set-up, which is presented in Figure 1. Experiments were carried out on a 2D granular medium, i.e. the motion of the grains was confined to a plane. The granular packing is constituted of metallic cylinders of millimetric size contained in a rectangular box made of two parallel glass plates, with an inner gap of thickness 3.4 mm, slightly larger than the height of the cylinders, $h = 3.00 \pm 0.01$ mm. The lateral walls of the box delimit a rectangular frame of height $H = 340$ mm and an adjustable width of typically $L = 300$ mm. We can change the distance between the lateral walls, i.e. the number of grains in 2D packing, to separate local behavior from collective behavior. The box is secured on a heavy plane able to be inclined at different rates ($5°$–$20°$ s^{-1}) so that we could set an arbitrary inclination angle θ from the horizontal. The angle of inclination θ is measured by means of a goniometer fixed to the plane. See Figure 1b for a sketch of this angle definition.

The cylinders of diameter $d = 6.00 \pm 0.05$ mm were used to prepare the monodisperse packings containing about 2400 grains. Disordered packings are prepared by pouring grains onto an initially horizontal glass plate at once. Then, they are spread until a flat layer is obtained, where the cylinders are randomly deposited without contact between them and at rest. The angle of the plane is then slowly increased up to the angle $\theta = 45°$ or $\theta = 85°$, at constant angular velocity. These final inclination angles correspond to a value larger than the static Coulomb angle of friction between the metallic grains and the glass plate, which is around $25°$. During the plane rotation, grains therefore freely slide downward and reach a mechanically

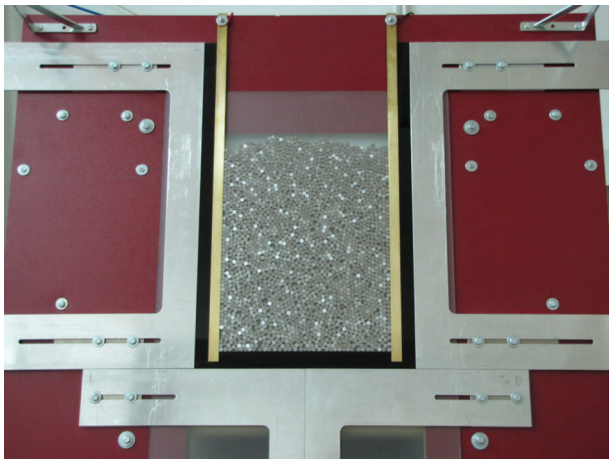

(a)

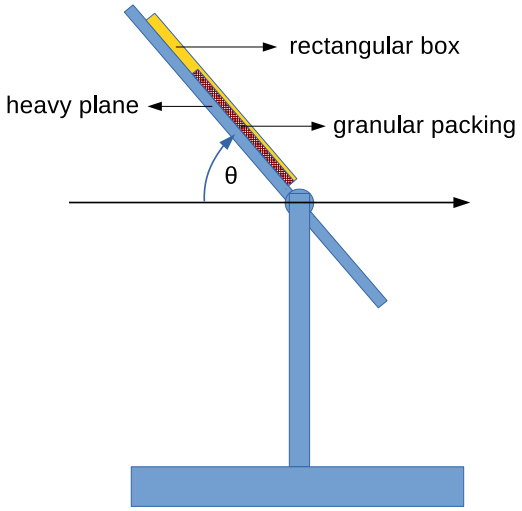

(b)

Fig. 1. (a) Photograph of the experimental setup. (b) Schematic diagram of the experimental setup (side view). The hatched area indicates the granular packing and θ is the inclination angle of the packing from the horizontal.

stable state. This way we control the balance of tangential and normal gravitational force on the layer and thus the contact network (and certainly also force network) inside the granular material. The measured packing fractions of these disordered packings are $\rho = 0.78{-}0.80 \pm 0.01$. Partially ordered packings are obtained by using the same initial procedure followed by the vibration of the inclined plane with a hammer-like device installed below the container. The packing fraction of densely packed systems is $\rho = 0.81{-}0.86 \pm 0.01$. Those densities are far from the close packing limit $\rho_{cp} = \pi/2\sqrt{3} \approx 0.91$ [21].

The bottom side of the rectangular box is electrically insulated. The current is injected to the packing side and not to only one grain. Long electrical contacts are disposed on two opposite lateral walls of the box. Electrical contacts are connected by cables to a Fluke 8008A Digital Multimeter which allows to measure the resistance. During

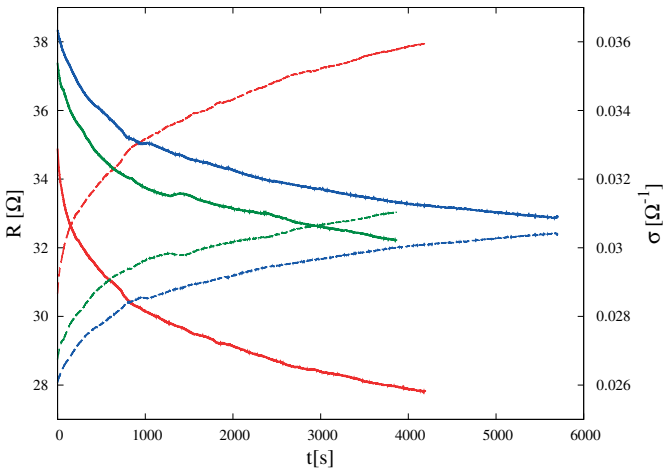

Fig. 2. Typical temporal evolutions of the resistance $R(t)$ obtained for an injected current $I = 1$ mA and an inclination angle $\theta = 85°$ (solid lines). The corresponding values of the conductance $\sigma(t)$ are given on the right axis (dashed lines). The different curves are obtained for several disordered packings prepared by using the same procedure.

the experiment, we have recorded the temporal evolution of the electrical resistance $R(t)$ of a metallic grains heap when a stable current flows through the system. A fixed current of $I = 1$ mA is injected during ∼20–100 min and the resistance $R(t)$ is sampled every 5 s. Different materials have been used for the electrodes (brass and stainless steel). We observed that the main relaxation features of conductance $\sigma(t)$ do not qualitatively depend on the electrode material. After each measurement of resistance $R(t)$, effective gravitational force on the grains is reduced to zero by placing the container in a horizontal position, and we rearrange the cylinders which creates new contacts for the next measurement.

The experimental setup has a high sensitivity to thermal perturbations and mechanical vibrations. It should be noted that we controlled the ambient humidity and temperature of the laboratory. The experimental reproducibility is qualitatively good although the exact values of conductance may exhibit fluctuations from one packing preparation to another.

3 Experimental results and discussion

In Figure 2, typical variations of the resistance $R(t)$ are shown versus time for an injected current $I = 1$ mA and an inclination angle $\theta = 85°$. Also included in Figure 2 is the temporal evolution of the conductance $\sigma(t)$ for the same experimental conditions. We observe that for the fixed injected current, the initial resistance for different packings differs from one another. This should be attributed to the changes in the contact network during the formation of new packings. It must be noted that the initial resistance dependence on the injected current in the range between 10 and 65 mA has been extensively analyzed in the experiments by Dorbolo et al. [14], that suggested that the initial

resistance decreases with the injected current. As seen in Figure 2, resistance $R(t)$ decreases very slowly with time for each packing. Our measurements have suggested that resistance $R(t)$ continues to decrease toward some saturation value. With the compacted (partially ordered) granular medium we made the same experiments and obtained qualitatively the same long-time behavior of the conductivity. Such behavior of the electrical conductivity, Dorbolo et al. [14] was demonstrated in the experiments at higher currents, 10 mA $\leqslant I \lesssim$ 25 mA.

Looking for a function that gives the best fit to the temporal evolution of the conductance $\sigma(t)$ in the case of very low injected currents $I \approx 10^{-3}$ A, we have obtained that the best agreement with our experimental data gives the Mittag-Leffler function. The fitting function we have used is of the form

$$\sigma(t) = \sigma_\infty - \Delta\sigma\, E_\alpha(-(t/\tau)^\alpha), \tag{1}$$

where σ_∞, $\Delta\sigma$, τ, and α are the fitting parameters. Parameter τ determines the characteristic time of the temporal evolution of conductance $\sigma = \sigma(t)$, and α measures the rate of conductance relaxation on this time scale. The parameter σ_∞ is the asymptotic value of the conductance $\sigma(t)$ when $t \to \infty$, and $\Delta\sigma = \sigma_\infty - \sigma(0)$.

In equation (1), E_α denotes the Mittag-Leffler function of order $\alpha \in (0, 1)$ [22]. It is defined through the inverse Laplace transform $\mathcal{L}$

$$E_\alpha\left[-(t/\tau)^\alpha\right] = \mathcal{L}\left[(u + \tau^{-\alpha}u^{1-\alpha})^{-1}\right], \tag{2}$$

from which the series expansion

$$E_\alpha\left[-(t/\tau)^\alpha\right] = \sum_{n=0}^{\infty} \frac{(-(t/\tau)^\alpha)^n}{\Gamma(1+\alpha n)}, \tag{3}$$

can be deduced; in particular, $E_1(-t/\tau) = \exp(-t/\tau)$. The Mittag-Leffler function interpolates between the initial stretched exponential form

$$E_\alpha\left[-(t/\tau)^\alpha\right] \sim \Phi_1(t) = \exp\left[-\frac{1}{\Gamma(1+\alpha)}(t/\tau)^\alpha\right], \quad t \ll \tau, \tag{4}$$

and the long-time power-law behavior

$$E_\alpha\left[-(t/\tau)^\alpha\right] \sim \Phi_2(t) = \frac{1}{\Gamma(1-\alpha)}(t/\tau)^{-\alpha}, \quad t \gg \tau. \tag{5}$$

In Figure 3 we compare the temporal evolution of the conductivity $\sigma(t)$ obtained when the experiment is performed for two different inclination angles of the plane, $\theta = 85°,\ 45°$. In the same figure the fits to the Mittag-Leffler law (Eq. (1)) are also given, demonstrating that it is excellently obeyed. The two fitting parameters are $\tau(85°) = 1.46 \times 10^4$ s, $\alpha(85°) = 0.461$ for $\theta = 85°$, and $\tau(45°) = 2.68 \times 10^5$ s, $\alpha(45°) = 0.327$ for $\theta = 45°$. In addition, the inset of Figure 3 compares the evolution of normalized conductivity $\sigma_r(t) = (\sigma(t) - \sigma(0))/(\sigma_\infty - \sigma(0)) = 1 - E[-(t/\tau)^\alpha]$ for the two values of inclination angle, $\theta = 85°,\ 45°$. It can be seen that the relaxation dynamics gets slower ($\tau(85°) < \tau(45°)$), and the evolution of the

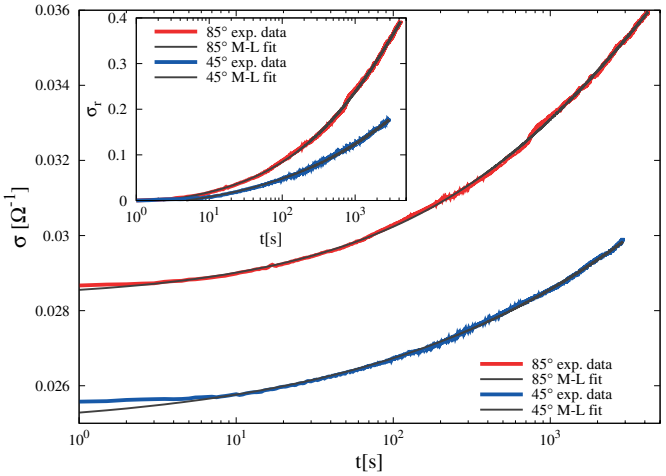

Fig. 3. Temporal evolution of the conductivity $\sigma(t)$ obtained for two different inclination angles of the plane, $\theta = 85°,\ 45°$. The thin (black) lines are the Mittag-Leffler fits of equation (1), with parameters $\tau(85°) = 1.46 \times 10^4$ s, $\alpha(85°) = 0.461$, and $\tau(45°) = 2.68 \times 10^5$ s, $\alpha(45°) = 0.327$. Inset: temporal evolution of the normalized conductance $\sigma_r(t) = (\sigma(t) - \sigma(0))/(\sigma_\infty - \sigma(0)) = 1 - E[-(t/\tau)^\alpha]$ for $\theta = 85°,\ 45°$.

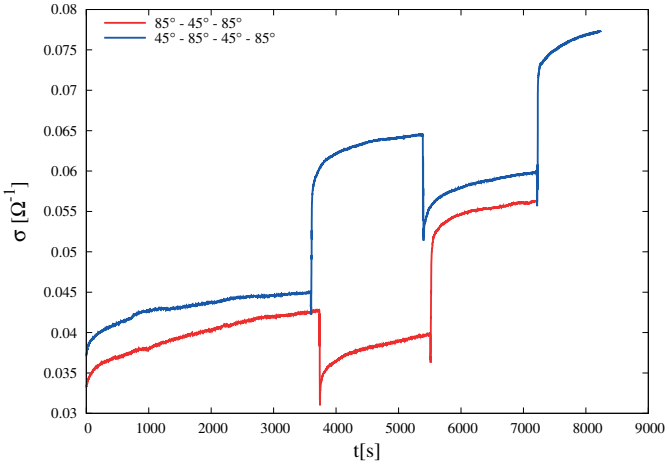

Fig. 4. Time evolution of the conductivity $\sigma(t)$ when the inclination angle θ is changed from $\theta_1 = 85°$ to $\theta_2 = 45°$ and vice versa in different time instants.

conductivity $\sigma(t)$ toward the saturation value takes place on much wider time scale ($\alpha(85°) > \alpha(45°)$) when the effective gravity $g_{\text{eff}} = g \sin\theta$ decreases.

Figure 4 shows the rapid variation of the electrical conductivity $\sigma(t)$ of granular packing induced by the abrupt change of the effective gravity $g_{\text{eff}} = g \sin\theta$. In this experiment, the inclination angle θ is changed from $\theta_1 = 85°$ to $\theta_2 = 45°$ and vice versa in three different time instants. For a sudden decrease in $g_{\text{eff}}(\theta_1) \to g_{\text{eff}}(\theta_2)$ it is observed that on short-time scales the conductivity σ decreases rapidly, while for a sudden increase in $g_{\text{eff}}(\theta_2) \to g_{\text{eff}}(\theta_1)$ the conductivity increases for short times. This behavior is transient, and after short time the usual increasing rate of conductivity $\sigma(t)$ growth is recovered. In addition, the rapid variation of the electrical conductivity induced

by a sudden change of the inclination angle θ is proportional to the angle change, $\Delta\theta = |\theta_1 - \theta_2|$ (not shown here).

Our findings for the behavior of the electrical conductivity, shown in Figures 3 and 4, clearly demonstrate that a granular material in the case of the higher values of effective gravity has a higher electrical conductivity. This is in agreement with experiments and numerical simulations examining the effect of gravity on the force network and microstructural properties of granular packings [23–27]. As gravity decreased, the spatial distribution of the force chain network changed from a dense, tangled network to one consisting of less tangled, longer chains. Intuitively, we would expect that shorter chains can support greater stress since there are fewer potential failure points. Thus, packings with more branching in their force chain network, induced by higher values of effective gravity are macroscopically stronger and more electrically conductive, since there are more pathways available for stress and electric current transmission.

Previously described "geometrical" contact disorder which arises from the lowering of the number of real contacts when the effective gravity decreases is not the sole cause that induces the abrupt changes of conductivity shown in Figure 4. Additionally, the "physical" contact disorder appears because some contacts are good transmitters, other are not. As the stress increases, some contacts may become active in turn, as the contact area may be cleaned of oxide coating or some other impurities. Consequently, the number of active contacts increases with the effective gravity. This effect contributes to the conductance due to the growth of the conducting network.

In order to better understand the reasons for the long term decay of the electric resistance, we have made the following experiment. The distance between the lateral walls of the box (electrodes) is reduced to $d(1+\sqrt{2})$. In this channel, six, nine or twelve disks are arranged to form square packing as illustrated in Figure 5a. This packing can easily be reproduced before each experiment. For the given configurations, each conductive path between the electrodes always includes only three disks. Therefore, the total number of possible conductive paths is equal to 5, 9, and 13, for configurations with 6, 9, and 12 disks, respectively. For configurations with small number of possible conductive paths, one should expect to detect abrupt changes in the resistance as a result of forming new conductive paths or termination of existing ones. However, Figure 5b shows that the resistance decreases continuously for all three configurations of disks. This means that the number of conductive paths does not change, but their conductivity increases over time. The fact that the decay of the resistance still holds for six disks (or five conductive paths), suggests that the origin of these changes is local. Consequently, long term resistance decay observed in the experiment is not related to large force chain rearrangements, but to individual microcontacts between two disks that rearrange.

It must be stressed that the time behavior of the conductance $\sigma(t)$ in experiments with reduced distance between the lateral walls (electrodes) is consistent with the

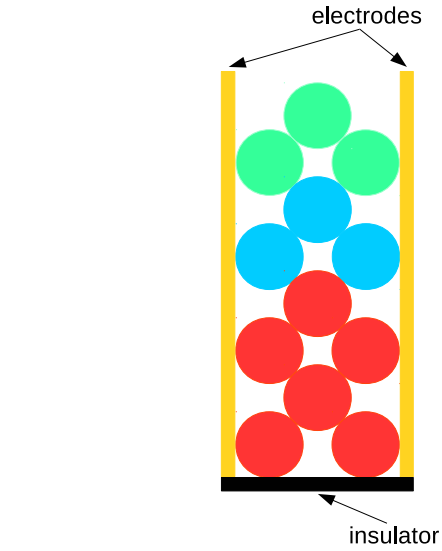

(a)

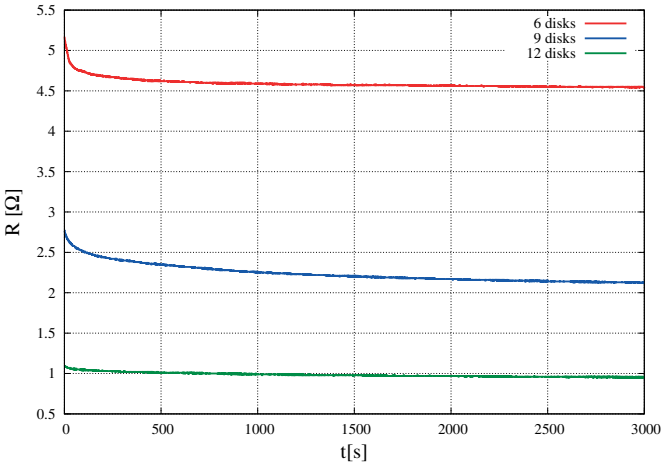

(b)

Fig. 5. Experiment with reduced distance between the lateral walls (electrodes). (a) Sketch of the 2D experimental setup. (b) Temporal evolutions of the resistance $R(t)$ obtained for configurations with 6, 9, and 12 disks shown on plot (a).

Mittag-Leffler law (1). According to equation (1), we get

$$\frac{\Delta\sigma(t)}{\Delta\sigma(0)} = \frac{\sigma_\infty - \sigma(t)}{\sigma_\infty - \sigma(0)} = E_\alpha(-(t/\tau)^\alpha). \qquad (6)$$

Temporal evolution of the quantity $\Delta\sigma(t)/\Delta\sigma(0)$ for the configuration with 9 disks (see Fig. 5) is shown in Figure 6 on double logarithmic scale together with the Mittag-Leffler fitting function $E_\alpha(-(t/\tau)^\alpha)$. In addition, Figure 6 shows the functions $\Phi_1(t)$ and $\Phi_2(t)$ (see Eqs. (4) and (5)) determined by fitting the conductance behavior $\sigma(t)$ to the Mittag-Leffler functional form (1).

The observed slow resistance decay might be related to the roughness of the surface of the disks. When two surfaces meet, and because no surface is perfectly smooth, asperity peaks or "a-spots" from each surface meet at the interface and form contact areas [3]. In this

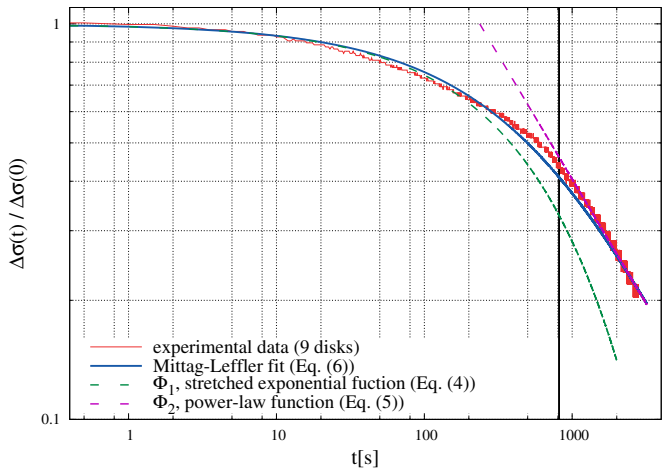

Fig. 6. Shown here is the double logarithmic plot of the temporal evolution of the normalized conductance deviation from the asymptotic value, $\Delta\sigma(t)/\Delta\sigma(0) = (\sigma_\infty - \sigma(t))/(\sigma_\infty - \sigma(0))$ (Eq. (6)). Data for $\sigma(t)$ are obtained for configuration with 9 disks in the experiment with reduced distance between the electrodes (Fig. 5). The solid (blue) line is the Mittag-Leffler function $E_\alpha(-(t/\tau)^\alpha)$, with parameters $\tau = 815.3$ s, $\alpha = 0.628$, and $\sigma_\infty = 0.497$. The dashed lines give the functions $\Phi_1(t)$ and $\Phi_2(t)$ (see Eqs. (4) and (5)), as indicated in the legend. The solid vertical line indicates the characteristic time $\tau = 815.3$ of the temporal evolution of conductance $\sigma(t)$.

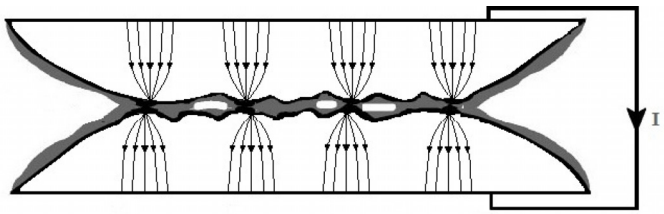

Fig. 7. Schematic diagram of current flow through a contact spot. The electrical connection between the two surfaces takes place at discrete solid spots, also known as a-spots or asperities, based on the roughness of the surfaces. These spots determine the true size of the contact area that can be as small as only a fraction of the nominal contact area.

way, when two disks are brought into contact, the surface irregularities of each disk create a large number of conducting micro-channels. The presence of the micro-contacts leads to a constriction of the current lines on tiny areas. Figure 7 shows a graphical representation of a contact area and contacting a-spots. Instead of passing uniformly through the oxide layer, electric current prefers to be divided in a large number of micro-currents following conducting micro-channels [2,3,11,13]. The convergence of the electrical current through the conducting a-spots is known as the constriction resistance or commonly the contact resistance [1]. With a small contact region comes a large contact resistance. Consequently, the flow of the current through the micro-contacts contributes to their heating by Joule effect and causes a softening or even melting some of them. At the same time, the mechanical stabilization of the discs, initiated by thermal perturbations,

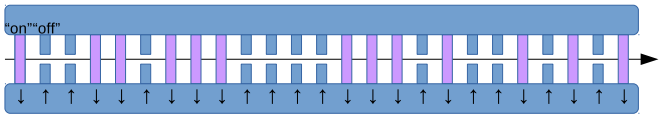

Fig. 8. Schematic picture of the dynamic model of the electric contact between two grains described in the text.

leads to the local micro-contact rearrangements at each disk, during which the new micro-contacts can be created. These electro-mechanical processes then allow both creation and breakdown of the micro-contacts between two disks. Adaptation of the micro-contacts to the flow of the electric current leads to a larger effective contact surface, thereby making the resistance of contact smaller.

4 Definition of the model and numerical simulation

Previous findings allow us to build a dynamic model of the electric contact between two grains that provides a very slow relaxation of electrical conductivity observed in the experiments. Our model can be regarded as a very simple picture of the interface between two metallic grains which is composed of a large number of micro-contacts. We consider a one-dimensional lattice, with N micro-contacts located at its lattice points (see Fig. 8). Each micro-contact can take two possible states, referred to as *"switched on"* ($\downarrow$) and *"switched off"* ($\uparrow$). A configuration of the contact is uniquely defined by N orientation variables $\{\Lambda_n | n = 1, \ldots, N\}$, with $\Lambda_n = +1$ denoting a micro-contact in state *"on"* ($\downarrow$), and $\Lambda_n = 0$ denoting a micro-contact in state *"off"* ($\uparrow$). To each micro-channel n in the state *"on"*, we assigned the same resistance, $r_n \equiv r^{(c)}$. When micro-channel n is in the state *"off"*, its resistance is too high and no current flows through it, so that we formally take $r_n = \infty$.

At first, we can try to model the contact interface, naively, by a continuous-time stochastic dynamics, described by the following general kinetic equations:

$$\frac{dp^{(\downarrow)}}{dt} = \omega_{\downarrow\uparrow} p^{(\uparrow)}(t) - \omega_{\uparrow\downarrow} p^{(\downarrow)}(t), \tag{7}$$

$$\frac{dp^{(\uparrow)}}{dt} = \omega_{\uparrow\downarrow} p^{(\downarrow)}(t) - \omega_{\downarrow\uparrow} p^{(\uparrow)}(t), \tag{8}$$

where $p^{(\uparrow)}(t)$ and $p^{(\downarrow)}(t)$ are the probabilities for finding the micro-contact in the states *"off"* and *"on"* at time t, respectively. Here, $\omega_{\downarrow\uparrow}$ and $\omega_{\uparrow\downarrow}$ represent, respectively, the constant transition probability rate from the state *"off"* to the state *"on"*, and from the state *"on"* to the state *"off"*. The term $\omega_{\downarrow\uparrow} p^{(\uparrow)}$ describes transition into the state *"on"* from the state *"off"*, and $\omega_{\uparrow\downarrow} p^{(\downarrow)}$ corresponds to transition out of the *"on"* into the other state *"off"*. Since the micro-channels of conduction are connected in parallel, the total contact conductance $\sigma(t) = 1/R(t)$ is expressed as the sum of their individual conductances

$\sigma_n = 1/r_n = 1/r^{(c)} \equiv \sigma^{(c)}$:

$$\sigma(t) = \sum_{n=1}^{N} \Lambda_n(t)\sigma^{(c)} = \sigma_{\max} p^{(\downarrow)}(t), \tag{9}$$

where $\sigma_{\max} = N\sigma^{(c)}$ is the conductance when all micro-contacts are in the state *"on"*. We have two limits: $p^{(\downarrow)} = 1$ when $\sigma = \sigma_{\max}$ (resistance is minimal) and $p^{(\downarrow)} = 0$ when $\sigma = 0$. Setting $\left.\frac{dp^{(\downarrow)}}{dt}\right|_{t\to\infty} = 0$ and $\left.\frac{dp^{(\uparrow)}}{dt}\right|_{t\to\infty} = 0$ in equations (7) and (8) they become a set of two algebraic equations whose solution provides the steady-state values of the conductance $\sigma(\infty)$:

$$\sigma(\infty) = \sigma_{\max} p^{(\downarrow)}(\infty) = \sigma_{\max}\frac{\omega_{\downarrow\uparrow}}{\omega}, \tag{10}$$

where $\omega = \omega_{\downarrow\uparrow} + \omega_{\uparrow\downarrow}$ is the total transition probability rate. This steady state will be reached by the system from any initial configuration. Assume that for $t = 0$:

$$p^{(\uparrow)}(0) = \frac{N^{(\uparrow)}(t=0)}{N}, \quad p^{(\downarrow)}(0) = \frac{N^{(\downarrow)}(t=0)}{N}, \tag{11}$$

where $N^{(\uparrow)}$ and $N^{(\downarrow)}$ are the number of micro-contacts in the states *"off"* and *"on"*, respectively. Without loss of generality we assume that for $t = 0$ the states *"off"* dominate, i.e. $N^{(\uparrow)}(t=0) > N^{(\downarrow)}(t=0)$. The solution of equations (7) and (8) with initial conditions (11) is straightforward. Accordingly, the conductance of the contact (Eq. (9)) grows exponentially in time towards the steady state value:

$$\sigma(t) = \sigma(\infty) - [\sigma(\infty) - \sigma(0)]\exp(-\omega t), \tag{12}$$

where $\sigma(0) = \sigma_{\max} p^{(\downarrow)}(0) = \sigma_{\max} N^{(\downarrow)}(t=0)/N$ is the conductance at the moment $t = 0$, when an electric current is turned on.

Not unexpectedly, this simplified model does not describe the behavior of a real electrical contact between metallic grains at low applied current, i.e. it is not a good approximation for the conduction dynamics. Our model requires substantial addition and extension in order to have the ability to properly capture the slow relaxation dynamics of conductivity observed in the experiments. The main physical idea of our approach is that the time intervals between the successive micro-contact closing/opening are governed by a certain waiting-time distribution $\psi(t)$. This function governs the *random time* intervals between single microscopic jumps *"on"* $(\downarrow) \leftrightarrow$ *"off"* $(\uparrow)$ of the micro-contacts. Actually, in our model the evolutions of the number of micro-contacts in the states *"on"* and *"off"* are subordinated by another random process. Random switching of micro-contacts between the states *"on"* and *"off"* are *parent* random processes $Y(t)$ in the sense of subordination (see Eqs. (7) and (8)). Recall that a subordinated process $Y[U(t)]$ is obtained by randomizing the time clock of a random process $Y(t)$ using a random process $U(t)$. The latter process is referred to as the randomized time. The new clock generalizes the deterministic time clock of the kinetic equation for the Markovian process (Eqs. (7) and (8)).

Now we consider in more details the evolution of the number of micro-contacts in the states *"on"* and *"off"*. These are *parent* random processes in the sense of subordination. Consider a sequence T_i, $i = 1, 2, \ldots$ of non-negative, independent, identically distributed random variables which represent the waiting time intervals between single microscopic jumps *"on"* $(\downarrow) \leftrightarrow$ *"off"* $(\uparrow)$ of the micro-contacts. If the waiting times T_i belong to the strict domain of attraction of an α-stable distribution $(0 < \alpha < 1)$, their sum $n^{-1/\alpha}\sum_{i=1}^{n} T_i$, $n \in N$ converges in distribution to a stable law with the same index α [17,28,29]. The continuous limit of the discrete counting process $\{N_t\}_{t\geq 0} = \max\{n \in N | \sum_{i=1}^{n} T_i \leq t\}$ is the hitting time process $S(t)$ (also called the first passage time). We choose the nondecreasing random process $S(t)$ for a new time clock (stochastic time arrow). The probability density of the process $S(t)$ has the following form [30]:

$$p_\alpha^S(t,\tau) = \frac{1}{2\pi j}\int_{\mathrm{Br}} u^{\alpha-1}\exp(ut - \tau u^\alpha)du = t^{-\alpha}F_\alpha\left(\frac{\tau}{t^\alpha}\right), \tag{13}$$

where Br denotes the Bromwich path and $j = \sqrt{-1}$. The function $F_\alpha(z)$ can be expanded as a Taylor series:

$$F_\alpha(z) = \sum_{k=0}^{\infty}\frac{(-z)^k}{k!\,\Gamma(1-\alpha-k\alpha)}, \tag{14}$$

where $\Gamma(\cdot)$ is the gamma function. The probability density $p_\alpha^S(t,\tau)$ determines the probability to be at the internal time (or so-called operational time) τ on the real time t [29,31].

The stochastic time arrow can be applied to the kinetic equations (7) and (8). Take the process $S(t)$ as a subordinator. It accounts for the amount of time when an micro-contact does not change its state. If $p^{(\downarrow)}(\tau)$ and $p^{(\uparrow)}(\tau)$, taken from equations (7) and (8) as probability laws of the parent process, depend now on the local time τ, then the resulting probabilities $p_\alpha^{(\downarrow)}(t)$ and $p_\alpha^{(\uparrow)}(t)$ after the subordination are determined by the integral relations

$$p_\alpha^{(\downarrow)}(t) = \int_0^\infty d\tau\; p_\alpha^S(t,\tau)p^{(\downarrow)}(\tau), \tag{15}$$

$$p_\alpha^{(\uparrow)}(t) = \int_0^\infty d\tau\; p_\alpha^S(t,\tau)p^{(\uparrow)}(\tau). \tag{16}$$

Now the relaxation of conduction $\sigma(t)$ is defined by two stochastic processes, random switching of micro-contacts and random waiting times between these events. The ratio of micro-contacts in the state *"off"* $(\uparrow)$ and another in the state *"on"* $(\downarrow)$ is subordinated by the process $S(t)$. In other words, the new relaxation process (Eqs. (15) and (16)) is obtained by randomizing the time clock of the continuous-time stochastic dynamics (Eqs. (7) and (8)) using the random process $S(t)$ [29,31]. The stochastic time clock has a clear physical sense. The electrical connection between the two surfaces takes place at discrete solid a-spots in random points of time.

The equation describing the present model takes the form similar to equations (7) and (8), but the derivatives of first order become fractional of order $0 < \alpha < 1$ determined by the index of the process $S(t)$. In the following, using properties of the stochastic time clock, we derive the corresponding master equation with the fractional derivative of time, along the lines of references [31–33]. Let us present equations (7) and (8) in compact form

$$\frac{d}{dt}\boldsymbol{p}(t) = \hat{\omega}\,\boldsymbol{p}(t), \tag{17}$$

where $\boldsymbol{p}(t) = \left[p^{(\downarrow)}(t)\; p^{(\uparrow)}(t)\right]^T$ and $\hat{\omega}$ denotes the transition rate operator:

$$\hat{\omega} = \begin{bmatrix} -\omega_{\uparrow\downarrow} & \omega_{\downarrow\uparrow} \\ \omega_{\uparrow\downarrow} & -\omega_{\downarrow\uparrow} \end{bmatrix}. \tag{18}$$

It is important to note that the operator $\hat{\omega}$ is independent of time. Equation (17) can be written in the integral form

$$\boldsymbol{p}(t) = \boldsymbol{p}(0) + \int_0^\infty d\tau\; \hat{\omega}\,\boldsymbol{p}(\tau). \tag{19}$$

The Laplace transform of equation (19) gives the relation

$$\hat{\omega}\,\tilde{\boldsymbol{p}}(s) = s\tilde{\boldsymbol{p}}(s) - \tilde{\boldsymbol{p}}(0), \tag{20}$$

where the Laplace transform $\mathcal{L}$ is defined as:

$$\mathcal{L}\boldsymbol{p}(t) \equiv \tilde{\boldsymbol{p}}(s) = \int_0^\infty dt\,\exp(-st)\boldsymbol{p}(t). \tag{21}$$

In the Laplace space the probabilities $\boldsymbol{p}_\alpha(t) = \left[p_\alpha^{(\downarrow)}(t)\; p_\alpha^{(\uparrow)}(t)\right]^T$ (see Eqs. (15) and (16)) take the most simple form

$$\tilde{\boldsymbol{p}}_\alpha(s) = s^{\alpha-1}\tilde{\boldsymbol{p}}(s^\alpha), \tag{22}$$

since $\tilde{p}_\alpha^S(s,\tau) = s^{\alpha-1}\exp(-\tau s^\alpha)$ [34]. When the operator $\hat{\boldsymbol{\omega}}$ acts on the Laplace image $\tilde{\boldsymbol{p}}_\alpha(s)$ (Eq. (22)), we obtain

$$\begin{aligned}\hat{\omega}\tilde{\boldsymbol{p}}_\alpha(s) &= s^{\alpha-1}\hat{\omega}\tilde{\boldsymbol{p}}(s^\alpha) = s^{\alpha-1}\left(s^\alpha\tilde{\boldsymbol{p}}(s^\alpha) - \tilde{\boldsymbol{p}}(0)\right) \\ &= s^\alpha\tilde{\boldsymbol{p}}_\alpha(s) - s^{\alpha-1}\tilde{\boldsymbol{p}}(0).\end{aligned} \tag{23}$$

The inverse Laplace transform $\mathcal{L}^{-1}$ of the latter expression (23) gives the abstract partial differential equation with the fractional derivative of time:

$$\boldsymbol{p}_\alpha(t) = \boldsymbol{p}(0) + {}_0D_t^{-\alpha}\hat{\omega}\,\boldsymbol{p}_\alpha(t). \tag{24}$$

Here we use the fractional Riemann-Liouville integral operator defined via the formula

$${}_0D_t^{-\alpha}f(t) = \frac{1}{\Gamma(\alpha)}\int_0^t d\tau\;(t-\tau)^{\alpha-1}f(\tau), \quad 0 < \alpha < 1, \tag{25}$$

with the convenient property $\mathcal{L}[{}_0D_t^{-\alpha}f(t)] = s^{-\alpha}\tilde{f}(s)$ [35]. Using equation (24) and taking into account that $\sigma(t) = \sigma_{\max}p_\alpha^{(\downarrow)}(t)$, we obtain that the deviation $\Delta\sigma(t) = \sigma(\infty) - \sigma(t)$ of the conduction $\sigma(t)$ from its steady-state value $\sigma(\infty)$ obeys the fractional differential equation

$$\Delta\sigma(t) = \Delta\sigma(0) - \omega\left[{}_0D_t^{-\alpha}\Delta\sigma(t)\right], \tag{26}$$

where $\omega = \omega_{\downarrow\uparrow} + \omega_{\uparrow\downarrow}$ is the total transition probability rate and $\sigma(\infty)$ is defined by equation (10). In equation (26), the fractional derivative on the rhs describes a process which is subordinated to the simple micro-contact switching; the subordination is defined by the α-stable waiting time distribution. By differentiating equation (26) with respect to time and with the help of the formula [35]

$$\frac{d}{dt}\,{}_0D_t^{-\alpha}f(t) = {}_0D_t^{1-\alpha}f(t), \tag{27}$$

it is found that

$$\frac{d}{dt}\Delta\sigma(t) = -\tau_r^{-\alpha}\,{}_0D_t^{1-\alpha}\Delta\rho(t), \tag{28}$$

where $\tau_r = \omega^{-1/\alpha} = (\omega_{\downarrow\uparrow} + \omega_{\uparrow\downarrow})^{-1/\alpha}$. Equation (28) is an integro-differential equation. The Riemann-Liouville operator ${}_0D_t^{1-\alpha}$ introduces a convolution integral with the power-law kernel $M(t) \propto t^{\alpha-2}$. The parameter τ_r may be interpreted as a generalized relaxation time. Indeed, the solution of equation (28) can be expressed in terms of the Mittag-Leffler function E_α of order α via [35,36]

$$\Delta\sigma(t) = \Delta\sigma(0)E_\alpha\left[-\left(\frac{t}{\tau_r}\right)^\alpha\right]. \tag{29}$$

Let us briefly describe the algorithm used in our numerical simulation. At each Monte Carlo step one lattice site is selected at random, and one of the two possible transitions between the two different states of the micro-contact is chosen at random. The choice of the transition from the state *"off"* to the state *"on"* occurs with probability $p_{\downarrow\uparrow}$, and from the state *"on"* to the state *"off"* with probability $p_{\uparrow\downarrow}$. The transition probabilities obey the normalization condition $p_{\downarrow\uparrow} + p_{\uparrow\downarrow} = 1$. When the attempted process is an *"off"* → *"on"* transition, and if randomly chosen micro-contact is in the *"off"* state, its state switches form *"off"* to *"on"*. On the contrary, if randomly chosen micro-contact is in the *"on"* state the attempt is abandoned. When the attempted process is an *"on"* → *"off"* transition, and provided that the selected micro-contact is in the *"on"* state, its state is changed from the *"on"* to *"off"*. Otherwise, we reject the switching trial. Switching processes at micro-contacts are assumed to happen instantaneously or at least in negligible time.

The random time τ between the successive micro-contact closing/opening attempts is extracted from a residence time distribution $\psi(\tau)$. We assume that the waiting-time intervals T_i between single microscopic jumps *"on"* $(\downarrow)$ ↔ *"off"* $(\uparrow)$ of the micro-contacts belong to the strict domain of attraction of an α-stable distribution $(0 < \alpha < 1)$ [17,28]. In that case, the probability that T_i is greater than some number $t > 0$ (tail probability) is asymptotically a power law, i.e. $P(T_i > t) \propto t^{-\alpha}$ as $t \to \infty$ [28]. Accordingly, decreasing of the parameter α in the range

$(0,1)$ increases the contribution of long waiting-time intervals T_i during the relaxation process. A suitable possible choice for a residence time distribution $\psi(\tau)$ is the Mittag-Leffler distribution defined by

$$\psi(\tau) = -\frac{d}{d\tau} E_\alpha(-(\tau/\nu)^\alpha), \tag{30}$$

where E_α is the Mittag-Leffler function of order $\alpha \in (0,1)$ and the constant ν is the time-scaling parameter. The basic role of the Mittag-Leffler waiting time probability density in the time fractional continuous time random walk (CTRW) has become well known by the seminal paper of Hilfer and Anton [37]. The probability density $\psi(\tau)$ for the waiting times can be numerically calculated by the series expansion (3). This method produces a pointwise representation of the density on a finite interval. Random numbers can then be produced by rejection, most efficiently with a look-up table and interpolation. More convenient is the following inversion formula by Kozubowski and Rachev [38,39]:

$$\tau = -\nu \ln u \left(\frac{\sin(\alpha\pi)}{\tan(\alpha\pi v)} - \cos(\alpha\pi) \right)^{1/\alpha}, \tag{31}$$

where $u, v \in (0,1)$ are independent uniform random numbers, ν is the scale parameter, and τ is a Mittag-Leffler random number. For $\alpha = 1$, equation (31) reduces to the inversion formula for the exponential distribution, i.e. $\tau = -\nu \ln u$. In each computational step the time t and the conductance σ are updated, $t \to t + \tau$ and $\sigma \to \sigma + \Delta\sigma$, where $\Delta\sigma \in \{\pm\sigma^{(c)}, 0\}$. Reiterating this algorithm, the full conductance growth above the initial value $\sigma(0) = \sigma_{\max} N^{(\downarrow)}(t=0)/N$ to the steady-state limit $\sigma(\infty)$ (Eq. (10)) can be computed.

The time-scaling parameter ν in equation (31) is calculated using the procedure detailed in references [40,41]. The quantities $\omega_{\downarrow\uparrow} = (p_{\downarrow\uparrow}/N)\nu^{-\alpha}$ and $\omega_{\uparrow\downarrow} = (p_{\uparrow\downarrow}/N)\nu^{-\alpha}$ in the fractional kinetic equation (28) are referred to as the fractional *"off"* $\to$ *"on"* and *"on"* $\to$ *"off"* rates. Using the normalization condition for the transition probabilities, i.e. $p_{\downarrow\uparrow} + p_{\uparrow\downarrow} = 1$, one obtains that

$$p_{\downarrow\uparrow} = \frac{\omega_{\downarrow\uparrow}}{\omega_{\downarrow\uparrow} + \omega_{\uparrow\downarrow}}, \quad p_{\uparrow\downarrow} = \frac{\omega_{\uparrow\downarrow}}{\omega_{\downarrow\uparrow} + \omega_{\uparrow\downarrow}}, \tag{32}$$

and

$$\nu = \left(N(\omega_{\downarrow\uparrow} + \omega_{\uparrow\downarrow})\right)^{-1/\alpha}. \tag{33}$$

In that case, the results of simulations are independent of the number of micro-contacts in the system. The fractional rates can be chosen as

$$\omega_{\downarrow\uparrow} = \omega \frac{1}{1+\gamma}, \quad \omega_{\uparrow\downarrow} = \omega \frac{\gamma}{1+\gamma}, \tag{34}$$

where $\gamma = p_{\uparrow\downarrow}/p_{\downarrow\uparrow}$. We impose that the parameter $\omega > 0$ in equation (34) depends only on the micromechanical properties of the contact, i.e. ω does not depend on the injected current I and the effective gravity $g_{\text{eff}} = g \sin\theta$ (an inclination angle θ of the plane) in the experiment. In fact, the form (34) of the fractional rates ensures that the total rate $\omega_{\downarrow\uparrow} + \omega_{\uparrow\downarrow} = \omega \neq f(\gamma)$ is independent on the parameter γ.

The crucial parameter which determines the final steady-state conductance $\sigma(\infty)$ and controls the dynamics, is the ratio $\gamma = p_{\uparrow\downarrow}/p_{\downarrow\uparrow} = \omega_{\uparrow\downarrow}/\omega_{\downarrow\uparrow}$. According to equation (10), the steady-state value of the conductivity $\sigma(\infty)$ is determined by

$$\sigma(\infty) = \sigma_{\max} \frac{1}{1+\gamma}. \tag{35}$$

The conductance $\sigma(\infty)$ is a decreasing function of the parameter $\gamma \geq 0$ and varies between 0 ($\gamma \to \infty$) and $\sigma_{\max}$ ($\gamma = 0$).

It is important to note that the coefficient α is not independent as far as its functional dependence on the parameter γ is concerned. We postulate that the parameters $0 < \alpha < 1$ and $\gamma > 0$ obey a simple relation:

$$\alpha = \frac{1}{1+\gamma}. \tag{36}$$

The value of parameter α decreases monotonically from unity as a function of the parameter γ. This relationship can be justified by the following phenomenological argument. Mapping the model on to the experiment, *"on"* $\to$ *"off"* event is associated with the opening of a micro-contact, whereas an *"off"* $\to$ *"on"* event is associated with the closing of a micro-contact. The number of micro-contacts in the state *"off"* and another in the state *"on"* is controlled by the parameter $\gamma = p_{\uparrow\downarrow}/p_{\downarrow\uparrow}$. Higher values of the effective gravity g_{eff} mean stronger interaction between the contact surfaces, thereby reducing the possibility of termination of micro-contacts, and stimulates the process of creating new ones. Therefore, it is acceptable to suppose that increasing the effective gravity g_{eff} corresponds to reduction of the parameter γ. Consequently, equation (35) indicates that the steady-state value of the conductivity $\sigma(\infty)$ increases with the increasing of the effective gravity g_{eff}. Furthermore, from equation (36) it follows that higher values of effective gravity are consistent with the greater values of the parameter α. Increasing of the parameter α in the range $(0,1)$ decreases the contribution of long waiting-time intervals T_i during the relaxation process, because $P(T_i > t) \propto t^{-\alpha}$ as $t \to \infty$ [28]. This causes that the relaxation dynamics gets faster when the effective gravity g_{eff} increases, in accordance with our experiment. Analogously, in the present model, parameter γ has higher values for the lower values of effective gravity g_{eff}. In addition, decreasing of the parameter α (Eq. (36)) increases the contribution of long waiting-time intervals T_i during the relaxation process. Accordingly, evolution of the conductivity $\sigma(t)$ toward saturation value takes place on much wider time scale when the effective gravity g_{eff} decreases, which is consistent with the results of the experiment. Now it can be concluded that the parameter γ within a model plays a role similar to that of the intensity of effective gravity g_{eff} in real experiments.

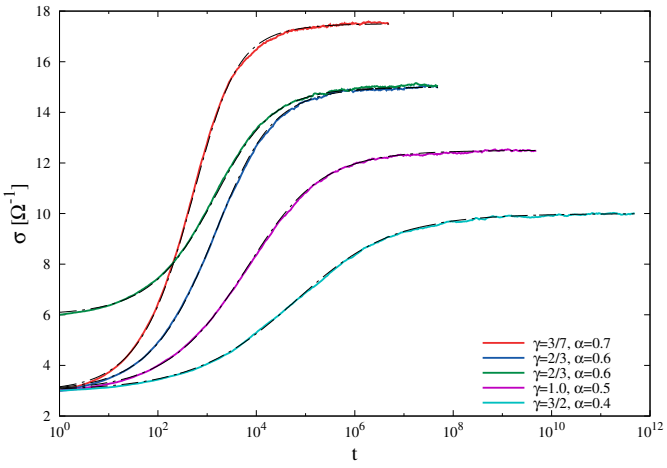

Fig. 9. Temporal evolution of the conduction $\sigma(t)$ obtained through Monte-Carlo simulations (solid lines) and analytically (dashed lines) for various values of parameter $\gamma = 3/7,\ 2/3,\ 1,\ 3/2$. Two curves, for the same value of $\gamma = 2/3$, demonstrate that the same steady-state will be reached by the system from any initial configuration.

The growth of a generalized relaxation time τ_r with γ can be accurately described by the exponential law:

$$\tau_r = \tau_0 \exp(\gamma_0 \cdot \gamma). \tag{37}$$

Indeed, inserting expressions $\gamma_0 = \ln(1/\omega) \neq f(\gamma)$ and $\tau_0 = 1/\omega \neq f(\gamma)$ into equation (37), and eliminating γ with the help of relation (36), we can obtain the expression for the generalized relaxation time, $\tau_r = \omega^{-1/\alpha}$ (see Eq. (28)).

Now, we present and discuss numerical results regarding the temporal evolution of the conductivity $\sigma(t)$. All numerical simulations were performed on a system of $N = 25$ micro-contacts. The parameter ω was chosen to be $\omega = 10^{-2}$. In order to sufficiently diminish statistical fluctuations, it is necessary to average over many independent runs for each value of the parameter γ. Therefore, curves of the $\sigma(t)$ relaxation reported here are averages of 10^4 independent simulations. A detailed description for the computation of the averages can be found in reference [40].

Variation of the conductance $\sigma(t)$ with time for several values of parameter γ is presented in Figure 9. We have observed that the relaxation of the conductance gets slower when the parameter γ increases. The simulation curves are in a good qualitative agreement with our experimental data, since the parameter γ has higher values for lower values of the effective gravity g_{eff}. Actually, for small values of the effective gravity we obtain higher values for the relaxation times τ and lower values of the asymptotic conductance $\sigma(\infty)$. In the same figure, the relaxation curves obtained analytically by equation (29) are also given, demonstrating that the Mittag-Leffler law (29) is excellently obeyed in our simulations. For very small values of γ, i.e. for high values of g_{eff}, there is a rapid approach to the asymptotic conductance $\sigma(\infty)$, and consequently the parameter α reaches a value close to 1 (see Eq. (36)). Since $E_\alpha[-(t/\tau_r)^\alpha] \to \exp(-t/\tau_r)$ when $\alpha \to 1$, the slow relaxation feature disappears in the regime of strong external forces.

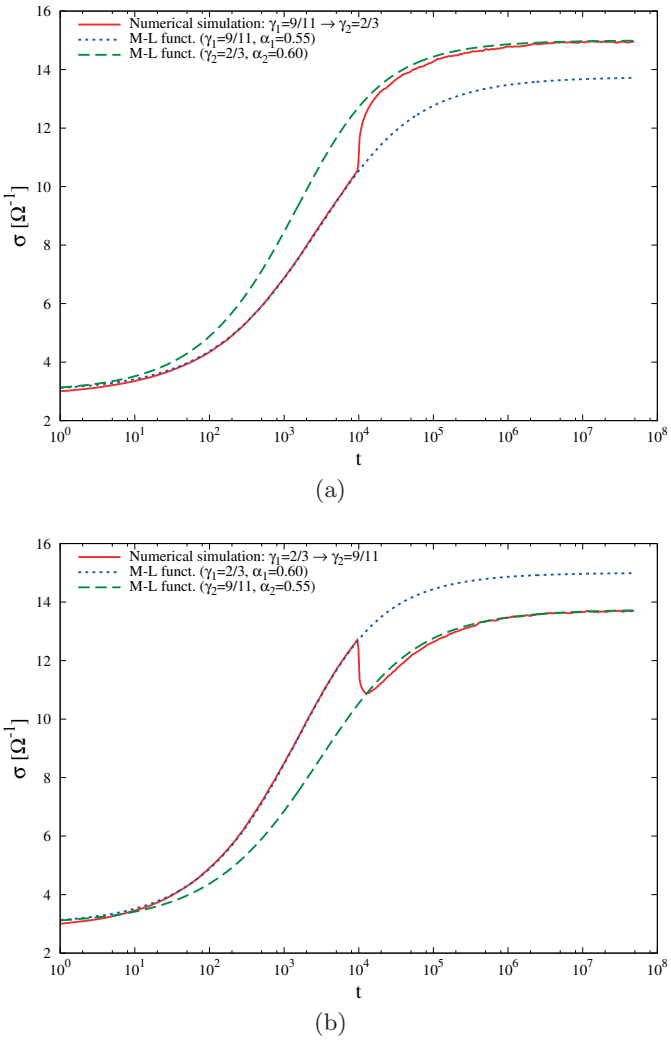

Fig. 10. Time evolution of the conductance $\sigma(t)$ when the parameter γ is switched (a) from $\gamma_1 = 9/11$ ($\alpha_1 = 0.55$) to $\gamma_2 = 2/3$ ($\alpha_2 = 0.60$) and (b) from $\gamma_1 = 2/3$ ($\alpha_1 = 0.60$) to $\gamma_2 = 9/11$ ($\alpha_2 = 0.55$), at a time $t_w = 10^4$ (solid curves). The dotted and dashed curves, obtained analytically by equation (29), correspond to the processes at constant γ_1 and γ_2.

Next we show that the proposed model reproduces qualitatively the rapid variation of the electrical conductivity $\sigma(t)$ of granular packing induced by the abrupt change of the effective gravity $g_{\text{eff}} = g \sin\theta$ (see Fig. 4). Since the parameter γ within a model plays a role similar to that of the intensity of the effective gravity g_{eff} in our experiment, we simulate the abrupt change of g_{eff} as an instantaneous change of the parameter γ in our model. Figure 10 shows a typical change of the electrical conductivity in our model after an abrupt change of the parameter γ. In Figure 10a the parameter γ is switched from $\gamma_1 = 9/11$ ($\alpha_1 = 0.55$) to $\gamma_2 = 2/3$ ($\alpha_2 = 0.60$) at $t_w = 10^4$. We observe that after the transient interval, the rapid growth of $\sigma(t)$ ceases and there is a crossover to the "normal" behavior, with relaxation rate becoming

the same as in the case of constant value of parameter γ. When $\gamma = p_{\uparrow\downarrow}/p_{\downarrow\uparrow}$ is abruptly lowered, the first effect is that the system tends to decrease the fraction of opened micro-contacts, so that conductance becomes larger. Therefore the rate of conductivity growth increases with respect to the unperturbed case. At larger times, however, the relaxation of $\sigma(t)$ is slowed down by the creation of smaller fraction of the micro-contacts that is available for transition from the state *"off"* to the state *"on"*. In Figure 10b we show the response of the system to instantaneous shift of parameter γ from $\gamma_1 = 2/3$ ($\alpha_1 = 0.60$) to $\gamma_2 = 9/11$ ($\alpha_2 = 0.55$) at a time $t_w = 10^4$. We observe an effect opposite to the previous case, i.e. we find that the conductance $\sigma(t)$ drops immediately following t_w. Both numerical results are qualitatively consistent with our experimental results shown in Figure 4.

5 Concluding remarks

We have reported experiments on the electrical conductivity in 2D packings of metallic disks at fixed injected current of $I = 1$ mA. This work provides experimental and theoretical additions to the studies of references [14,15] mostly carried out in the regime of higher currents ($I >$ 10 mA). The scenario of the evolution of the conductance depends on both the injected current and external forces acting on the packing. In this paper, we have attempted to give some insights into the mechanisms by which granular materials handle slow relaxation of electrical conductivity in the regime of very low injected currents and without external load.

We have experimentally investigated the conductance of 2D packings of metallic disks for different values of the effective gravity g_{eff}. We have shown that evolution of the conductivity $\sigma(t)$ toward saturation value takes place on much wider time scale when the effective gravity g_{eff} decreases. We have fitted the time dependences of the conductance $\sigma(t)$ with the Mittag-Leffler function (1). The characteristic timescale τ (Eq. (1)) is found to grow when the effective gravity g_{eff} decreases. By changing both the distance between the electrodes and the number of grains in the packing, it was shown that the long-term resistance decay observed in the experiment is not related to large force chain rearrangements, but to individual micro-contacts between two disks that rearrange. Hence, this long-term decay seems to be related to the enhancement of the contacts themselves. The behavior of granular material is thus completely different from a metallic bulk material. When the current is switched on, the metallic wire produces heat. This change in temperature makes the electrical conductance decrease. On the other hand, in the case of granular material, the opposite effect occurs. The local micro-contact rearrangements at each grain influence the conduction by increasing it. Consequently, in the case of granular material with weak links between conductive grains, electrical measurements have to be carefully implemented. The intensity of the injected current, external load and surface state of grains are seen to be relevant parameters.

These results were used as a basis for building of a dynamic model of the electric contact between two grains which is composed of a large number of micro-contacts. Actually, we have developed an artificial, but instructive model of a contact which can be regarded as a very simple picture of the interface between two metallic grains. We impose that the micro-contacts at the interface switch stochastically between the two states (*"on"* and *"off"*). By appropriately choosing this random process, one can provide the essential ingredients in our model to reproduce the slow relaxation of the electrical conductivity and mimic the rapid variation of the conductance $\sigma(t)$ induced by the abrupt change of the effective gravity g_{eff}. We think that the success of the model in emulating the experiments indicates that the dominant physical mechanisms have been correctly identified. Even though the model is simple enough as to be analytically tractable, the theoretical results are corroborated by numerical simulations of the corresponding stochastic fractional processes.

This work was supported by the Ministry of Education, Science, and Technological Development of the Republic of Serbia under projects ON171017, III45016, and by the European Commission under H2020 project VI-SEEM, Grant No. 675121. Numerical simulations were run on the PARADOX supercomputing facility at the Scientific Computing Laboratory of the Institute of Physics Belgrade.

Author contribution statement

Study conception and design: S.B. Vrhovac and Z.M. Jaksic; Acquisition of data: Z.M. Jaksic, M. Cvetkovic, and J.R. Scepanovic; Analysis and interpretation of experimental data: Z.M. Jaksic, M. Cvetkovic, and J.R. Scepanovic; Development of the theoretical formalism and analytic calculations: S.B. Vrhovac, Lj. Budinski-Petkovic, and I. Loncarevic; Development of the numerical simulations: S.B. Vrhovac, Lj. Budinski-Petkovic, and I. Loncarevic; Drafting of manuscript: S.B. Vrhovac and Lj. Budinski-Petkovic; Critical revision: S.B. Vrhovac, Lj. Budinski-Petkovic, and I. Loncarevic.

References

1. R. Holm, *Electric Contacts: Theory and Applications*, 4th edn. (Springer-Verlag, Berlin/Heidelberg, 1967)
2. V. Da Costa, Y. Henry, F. Bardou, M. Romeo, K. Ounadjela, Eur. Phys. J. B **13**, 297 (2000)
3. B.F. Toler, R.A. Coutu Jr., J.W. McBride, J. Micromech. Microeng. **23**, 103001 (2013)
4. E. Branly, C. R. Acad. Sci. **280**, 785 (1890)
5. S. Dorbolo, M. Ausloos, N. Vandewalle, Phys. Rev. E **67**, 040302 (2003)
6. E. Falcon, B. Castaing, C. Laroche, Europhys. Lett. **65**, 186 (2004)
7. E. Falcon, B. Castaing, Am. J. Phys. **73**, 302 (2005)
8. S. Dorbolo, N. Vandewalle, Traffic Granul. Flow **5**, 521 (2005)
9. P. Bèquin, V. Tourant, Granul. Matter **12**, 375 (2010)

10. M. Creyssels, S. Dorbolo, A. Merlen, C. Laroche, B. Castaing, E. Falcon, Eur. Phys. J. E **23**, 255 (2007)
11. E. Falcon, B. Castaing, M. Creyssels, Eur. Phys. J. B **38**, 475 (2004)
12. N. Vandewalle, C. Lenaerts, S. Dorbolo, Europhys. Lett. **53**, 197 (2001)
13. D. Bonamy, L. Laurent, Ph. Claudin, J.-Ph. Bouchaud, Europhys. Lett. **51**, 614 (2000)
14. S. Dorbolo, M. Ausloos, N. Vandewalle, M. Houssab, J. Appl. Phys. **94**, 7835 (2003)
15. J.J. Lee, C.W. Lee, I. Yu, Y.K. Jung, J. Lee, J. Phys.: Condens. Matter **19**, 356202 (2007)
16. R. Hilfer, J. Non-Cryst. Solids **305**, 122 (2002)
17. M.M. Meerschaert, H.-P. Scheffler, J. Appl. Probab. **41**, 623 (2004)
18. A.A. Stanislavsky, Phys. Rev. E **61**, 4752 (2000)
19. R. Metzler, J. Klafter, Phys. Rep. **339**, 1 (2000)
20. G.M. Zaslavsky, Phys. Rep. **371**, 461 (2002)
21. T. Aste, J. Phys.: Condens. Matter **17**, S2361 (2005)
22. E.W. Weisstein, Mittag-Leffler function, From MathWorld – A Wolfram Web Resource (2017), http://mathworld.wolfram.com/Mittag-LefflerFunction.html
23. D. Howell, R.P. Behringer, C. Veje, Phys. Rev. Lett. **82**, 5241 (1999)
24. M. Muthuswamy, A. Tordesillas, in *Proceedings of the 10th ASCE Aerospace Division International Conference on Engineereng, Construction and Operations in Challenging Environments (Earth & Space 2006)*, edited by R.B. Malla, W.K. Binienda, A.K. Maji (Aerospace Division of the American Society of Civil Engineers, Reston, VA, 2006), p. 33
25. M. Muthuswamy, A. Tordesillas, JSTAT **P09003** (2006)
26. A. Modaressi, S. Boufellouh, P. Evesque, Chaos **9**, 523 (1999)
27. Z.M. Jakšić, J.R. Šćepanović, I. Lončarević, Lj. Budinski-Petković, S.B. Vrhovac, A. Belić, Phys. Rev. E **90**, 062208 (2014)
28. A. Janicki, A. Weron, Stat. Sci. **9**, 109 (1994)
29. M. Magdziarz, K. Weron, Physica A **367**, 1 (2006)
30. F. Mainardi, Chaos Solitons Fract. **7**, 1461 (1996)
31. A.A. Stanislavsky, Phys. Rev. E **67**, 021111 (2003)
32. A.A. Stanislavsky, Chaos Solitons Fract. **34**, 51 (2007), in Search of a Theory of Complexity
33. Aleksander Stanislavsky, Karina Weron, Aleksander Weron, Commun. Nonlinear Sci. Numer. Simul. **24**, 117 (2015)
34. A.A. Stanislavsky, Acta Phys. Polonica B **34**, 3649 (2003)
35. F. Mainardi, R. Gorenflo, J. Comput. Appl. Math. **118**, 283 (2000)
36. R.K. Saxena, A.M. Mathai, H.J. Haubold, Physica A **344**, 657 (2004)
37. R. Hilfer, L. Anton, Phys. Rev. E **51**, R848 (1995)
38. T.J. Kozubowski, S.T. Rachev, J. Comput. Anal. Appl. **1**, 177 (1999)
39. D. Fulger, E. Scalas, G. Germano, Phys. Rev. E **77**, 021122 (2008)
40. E. Heinsalu, M. Patriarca, I. Goychuk, G. Schmid, P. Hänggi, Phys. Rev. E **73**, 046133 (2006)
41. E. Heinsalu, M. Patriarca, I. Goychuk, P. Hänggi, J. Phys.: Condens. Matter **19**, 065114 (2007)